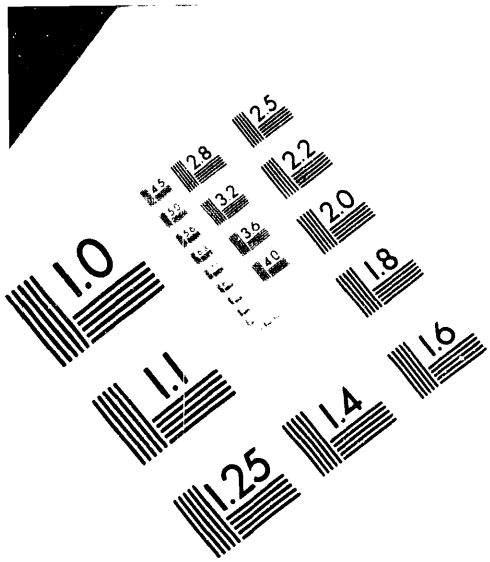

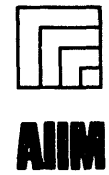

Association for Information and Image Management
1100 Wayne Avenue, Suite 1100
Silver Spring, Maryland 20910
301/587-8202

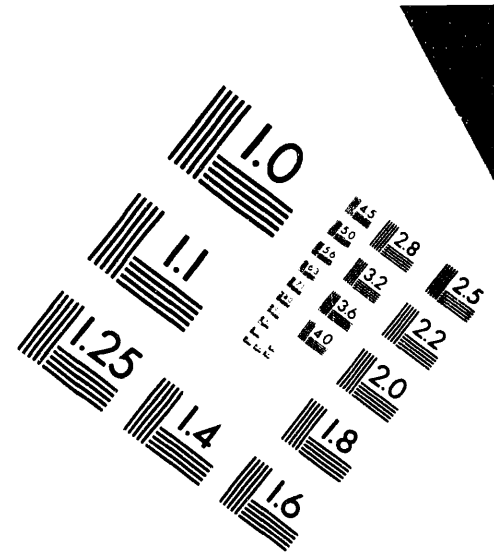

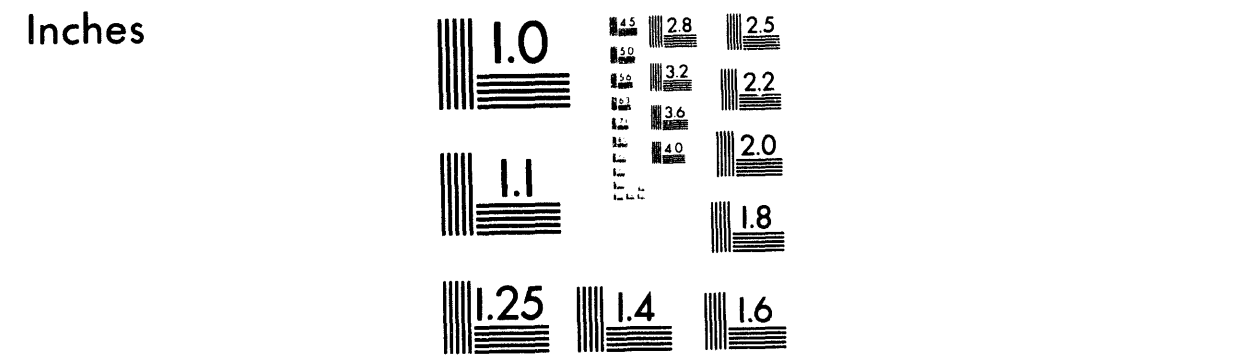

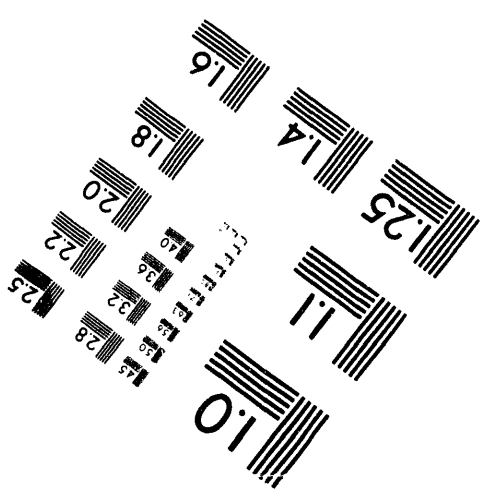

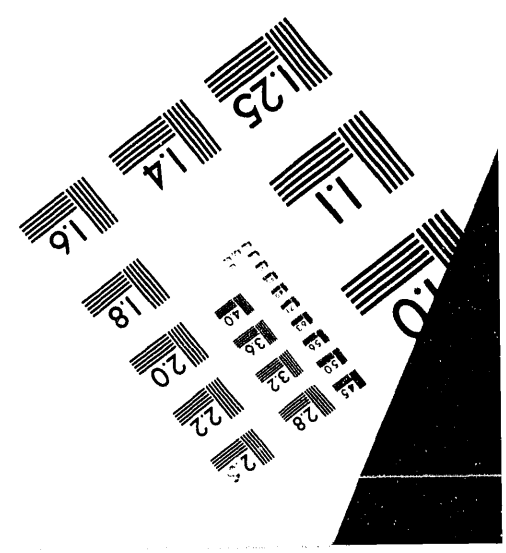

MANUFACTURED TO AIIM STANDARDS
BY APPLIED IMAGE, INC.

1 of 1

Distribution
Category UC-722

SAND92-2401
TTC1239
Unlimited Release
Printed March 1993

USE OF A COMMERCIAL HEAT TRANSFER CODE TO PREDICT HORIZONTALLY ORIENTED SPENT FUEL ROD SURFACE TEMPERATURES

S. D. Wix, Gram, Inc.*
Albuquerque, NM 87112

J. A. Koski, Sandia National Laboratories**
Albuquerque, NM 87185

* This work performed at Sandia National Laboratories, Albuquerque, New Mexico, supported by the U.S. Department of Energy under Contract DE-AC04-76DP00789.
**A United States Department of Energy facility.

ABSTRACT

A comparison between numerical calculations using commercial thermal analysis software packages and experimental data simulating a horizontally oriented spent fuel rod array was performed. Twelve cases were analyzed using air and helium for the fill gas, with three different heat dissipation levels. The numerically predicted temperatures are higher than the experimental data for all levels of heat dissipation with air as the fill gas. The temperature differences are 4°C and 23°C for the low heat dissipation and high heat dissipation, respectively. The temperature predictions using helium as a fill gas are lower for the low and medium heat dissipation levels, but higher at the high heat dissipation. The temperature differences are 1°C and 6°C for the low and medium heat dissipation, respectively. For the high heat dissipation level, the temperature predictions are 16°C higher than the experimental data.

Differences between the predicted and experimental temperatures can be attributed to several factors. These factors include experimental uncertainty in the temperature and heat dissipation measurements, actual convection effects not included in the model, and axial heat flow in the experimental data.

This work demonstrates that horizontally oriented spent fuel rod surface temperature predictions can be made using existing commercial software packages. This work also shows that end effects will be increasingly important as the amount of dissipated heat increases.

CONTENTS

FIGURES

Figure

TABLES

Table

1.0 INTRODUCTION

Radioactive spent fuel assemblies are a source of hazardous waste that will have to be dealt with in the near future. It is anticipated that the spent fuel assemblies will be transported to disposal sites in spent fuel transportation casks. In order to design a reliable and safe transportation cask, the maximum cladding temperature of the spent fuel rod arrays must be calculated. The maximum rod cladding temperature is a limiting factor in the amount of spent fuel that can be loaded in a transportation cask.

The scope of this work is to demonstrate that reasonable and conservative spent fuel rod surface temperature predictions can be made using commercially available thermal analysis codes. The demonstration is accomplished by a comparison between numerical temperature predictions, with a commercially available thermal analysis code, and experimental temperature data for electrical rod heaters simulating a horizontally oriented spent fuel rod bundle.

An emissivity sensitivity study was performed using the thermal model developed in this effort. The objective of the emissivity sensitivity study was to provide useful data on the relationship between rod and boundary emissivity and maximum rod surface temperature.

2.0 TECHNICAL DISCUSSION

2.1 Analysis Software

The analysis software consists of PATRAN,[1] a pre- and post-processing code used to create model geometries, apply boundary conditions, and display results; a code that calculates radiation view factors; Q/TRAN,[1] the thermal solver; and a material property database.

In an earlier work by Glass et al.,[2] six benchmark problems and their corresponding analyses were reported. Of the six problems, four were solved using Q/TRAN. One of the benchmarking problem geometries, UK-1, resembles the geometry modeled in this effort. UK-1 simulates a 16 x 16 array of heated and unheated pins in fuel and control rod locations. This configuration represents a PWR fuel element in a gas environment. The results of the UK-1 benchmark comparison show a maximum deviation of 6 percent between any of the four codes used to analyze the problem. The overall benchmarking results showed that the Q/TRAN results were within 10 percent of analytical and experimental solutions. These results provided confidence that Q/TRAN can be used in solving horizontally oriented spent fuel rod array heat transfer problems.

2.2 Experimental Data

The experimental data was taken in 1991 by Lovett and Todreas.[3] Their experiment was designed to characterize the heat transfer mechanisms in a dry, horizontally oriented nuclear spent fuel assembly. The components used in the experiments were designed to emulate a dry, horizontally oriented 8 x 8 boiling water reactor spent fuel assembly and its containment in a transportation cask. The equipment consisted of an 8 x 8 array of 0.62-meter-long heaters; an aluminum box used to define boundary conditions; a pressure vessel; and instrumentation for measuring temperature and heat dissipation. The heater rods were placed inside the aluminum box and the rod-box assembly was placed inside the pressure vessel. The pitch to diameter ratio of the heater rods was approximately 1.33. The experimental equipment used by Lovett and Todreas [3] was painted with black Krylon high heat spray paint; therefore, the emissivity could be approximated at 0.9.

Type K thermocouples were used to measure the heater rod centerline temperatures. These thermocouples were calibrated in-house using a reference standard calibrated to NIST standards. The temperature measurement tolerance for the thermocouples was ± 1.8°C.

An error analysis of the test data was performed by Lovett and Todreas.[3] The uncertainty in the total power measurement was calculated for a low power and a high power case. The calculated uncertainties are 2.4 watts and 10.4 watts for the low power and high power cases, respectively. The uncertainty in the temperature difference of the hottest heater rod and boundary box average wall temperature was also calculated. For the data used in this work, the temperature difference uncertainty was 2.55C°.

Their experiment consisted of setting the controller temperature for a given set of constraints, such as fill gas type and pressure, and then recording heater rod centerline temperatures and total heat dissipation when the system came to equilibrium. Four fill gases (air, helium, nitrogen, and argon) were used. Multiple heat dissipation cases were considered for each fill gas.

2.3 Thermal Model Description

Two-dimensional, finite-difference thermal models were developed for an array of sixty-four horizontal heated rods in a rectangular cavity. The geometry was based on a two-dimensional cross section of experimental equipment used by Lovett and Todreas.[3] Figure 1 presents a pictorial representation of the finite difference model used to simulate the Lovett and Todreas experiment. The boundary box represents the inside surface of the transportation cask.

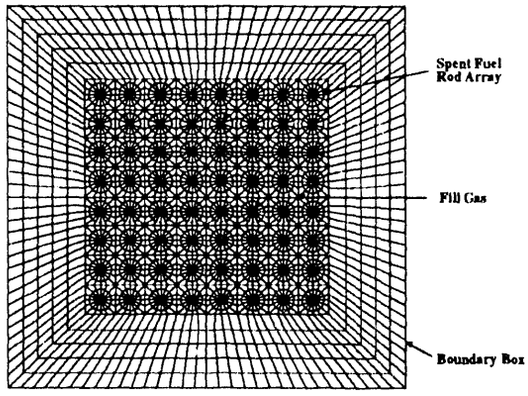

Figure 1. Thermal Model of a Spent Fuel Rod Array

Temperature boundary conditions for the boundary box were taken from their experimental data. Each model consisted of 2,241 nodes. All thermal simulations were steady state.

2.3.1 Thermal Model Approaches

Two thermal modeling approaches were used to predict steady-state temperatures in the simulated fuel assembly. The first approach was to construct a thermal model where the heat transfer mechanism was primarily radiation. Conduction through the fill gas was included in this approach and provided a second, although a less significant, heat transfer path. In the second approach, "convection quad" elements were included in the model to allow for natural convection boundary conditions at internal surfaces. This approach allows for some spatial variation of temperature in the fluid but does not include mass transfer effects because Q/TRAN does not solve the mass flow calculations necessary for natural convection problems. Both approaches used the same geometry. In the following discussion we will refer to the first approach as the radiation conduction case and the second approach as the radiation convection case.

The fill gas, which is used in actual transportation casks as a means of accentuating heat transfer and reducing potential oxidation problems with the cladding, was varied in the thermal calculations. Both modeling approaches were applied to one case where the fill gas was air, and a second case where the fill gas was helium. Air, which is not normally used as a fill gas due to potential cladding oxidation, was chosen because of the poor thermal conductivity when compared to other types of fill gases. Helium was chosen because of its relatively high thermal conductivity. A large range of potential fill gases is bracketed by these choices.

Other assumptions in the modeling are a constant and uniform surface emissivity, and the horizontal orientation of the rods. An emissivity of 0.9, which matched the emissivity published by Lovett and Todreas,[3] was used in the thermal calculations.

2.3.2 Boundary Conditions

Thermal boundary conditions used to calculate rod surface temperatures were taken from the experimental data. The boundary conditions in the thermal model consisted of radiation, heat sources, temperature, and convection. A radiation boundary condition was applied to each rod and the inside of the boundary box. Code was used to determine radiation view factors and calculate radiosity nodes and radiation conductors.

Heat sources were applied to each rod in the array. The rod material had a high thermal conductivity to minimize any temperature gradients within the rod. Because the two-dimensional model assumes a unit depth of 1 meter, and the heater rods used in Lovett and Todreas experiment were 0.62 meters long, the heat dissipation data from Lovett and Todreas were divided by the rod length to determine the heat dissipation per unit length. The heat dissipation per unit length was used in the thermal calculations.

Fixed temperature boundary conditions were applied to the outside of the boundary box. The model temperature boundary location matches the location of the boundary box experimental temperature data. Since the experimental data was for a quasi steady-state case, the model temperature boundary condition was not varied with respect to time.

Convection boundary conditions were applied to the rods and inside of the boundary box for the radiation convection case. Only the correlations available in the convection library in the commercial code were considered. The correlations chosen were the closest to describing the actual natural convection boundary condition, given the choices in the commercial code convection library. The corellations used to describe the natural convection boundary condition of the rods were

$$Nu = 0.53\ Ra^{0.25} \qquad 1E4 < Ra < 1E9 \tag{1}$$

$$Nu = 0.13\ Ra^{0.333} \qquad 1E9 < Ra < 1E12 \tag{2}$$

where

Nu = Nusselt number, and
Ra = Rayleigh number.

These equations are for the average heat transfer film coefficient from a single horizontal cylinder in an infinite medium.

The correlations used to calculate the natural convection boundary condition on the vertical walls of the boundary box were

$$Nu = 0.68 + (0.67Ra^{0.25})/(1+(0.492/Pr)^{0.5625})^{0.4444} \quad (3)$$

$$Nu = (0.825 +(0.387Ra^{0.1667})/(1+(0.492/Pr)^{0.5625})^{0.2963})^{2.0} \quad (4)$$

The correlations used to calculate the natural convection film coefficient on the upper interior surface of the boundary box were

$$Nu = 0.54\ Ra^{0.25} \qquad 2.6E4 < Ra < 1E7 \quad (5)$$

$$Nu = 0.15\ Ra^{0.333} \qquad 1E7 < Ra < 3E10 \quad (6)$$

The correlation used to calculate the natural convection film coefficient on the lower interior surface of the boundary box was

$$Nu = 0.27\ Ra^{0.25} \qquad 3E5 < Ra < 3E10 \quad (7)$$

The code bases material property evaluations on the film temperature. Details on the derivation of equations 1 through 6 are in references 1 and 4.

2.4 Calculated Data

The procedure for calculating rod surface temperatures and the procedure used in the emissivity sensitivity study are presented in this section.

2.4.1 Steady-State Rod Surface Temperature Calculations

Rod surface temperatures were calculated for twelve cases: six for the radiation conduction case and six for the radiation convection case. The radiation conduction and radiation convection cases were divided into three subcases for each type of fill gas. Each subcase had a unique heat dissipation and temperature boundary condition. Table 1 presents the cases.

Table 1

Thermal Model Cases and Boundary Conditions

Case	Fill Gas	Thermal Model	Heat Dissipation (W/m)	Temperature Boundary Condition Top (C)	RW (C)	Bottom (C)	LW (C)
1	Air	Rad. Cond.	51.3	46.6	46.4	45.0	46.2
2	Air	Rad. Cond.	232.4	84.9	84.8	80.8	83.7
3	Air	Rad. Cond.	627.2	143.6	143.8	136.3	141.6
4	Helium	Rad. Cond.	109.8	48.4	47.6	47.4	47.5
5	Helium	Rad. Cond.	425.8	97.0	94.1	93.8	93.9
6	Helium	Rad. Cond.	939.5	132.4	127.4	127.2	127.2
7	Air	Rad. Conv.	51.3	46.6	46.4	45.0	46.2
8	Air	Rad. Conv.	232.4	84.9	84.8	80.8	83.7
9	Air	Rad. Conv.	627.2	143.6	143.8	136.3	141.6
10	Helium	Rad. Conv.	109.8	48.4	47.6	47.4	47.5
11	Helium	Rad. Conv.	425.8	97.0	94.1	93.8	93.9
12	Helium	Rad. Conv.	939.5	132.4	127.4	127.2	127.2

2.4.2 Emissivity Study Calculations

Case 3 in Table 1 was used in the emissivity sensitivity study. The case chosen used a radiation conduction approach with high heat dissipation and an air fill gas. This case was chosen for three reasons. The low thermal conductivity of air minimizes conduction heat transfer through the fill gas. The radiation conduction approach eliminates convection effects. The high heat dissipation maximizes radiation heat transfer. By maximizing radiation heat transfer, minimizing conduction and eliminating convection heat transfer, emissivity sensitivity is maximized.

Temperatures were calculated using the thermal model for emissivities of 0.7, 0.8, 0.9, and 1.0. The only variable changed between each calculation was the rod and inside boundary box emissivity. Radiosity nodes and conductors were recalculated using the view factor code.

3.0 RESULTS

A comparison of the calculated temperatures to the experimental data and the maximum rod surface temperature as a function of emissivity is discussed in this section. Figures 2 and 3 present the experimental and calculated maximum rod surface temperatures for the air and helium fill gases, respectively. Figure 4 presents the emissivity versus maximum rod surface temperature relationship for Case 1. Figures A1 through B6 present a side-by-side comparison of experimental and calculated temperature contours. Figures A1 through A3 and A4 through A6 present temperature contour plots with an air fill gas for the radiation conduction and radiation convection cases, respectively. Figures B1 through B3 and B4 through B6 present temperature contour plots with a helium fill gas for the radiation conduction and radiation convection cases, respectively.

3.1 Air Fill Gas

As shown in Figure 2, the maximum rod surface temperatures for the lowest heat dissipation, 51.3 W/m, are 73.0C° from the experiment, in comparison with 78.9°C for the radiation conduction case, and 77.7°C for the radiation convection case. For medium heat dissipation, 232.4 W/m, the maximum rod surface temperatures are 154.8°C for the experiment 163.7°C for the radiationconduction case, and 162.7°C for the radiation convection case. For the highest heat dissipation, 627.3 W/m, the maximum rod surface temperatures are 256.3°C for the experiment, 279.2°C for the radiation conduction case, and 274.1°C for the radiation convection case.

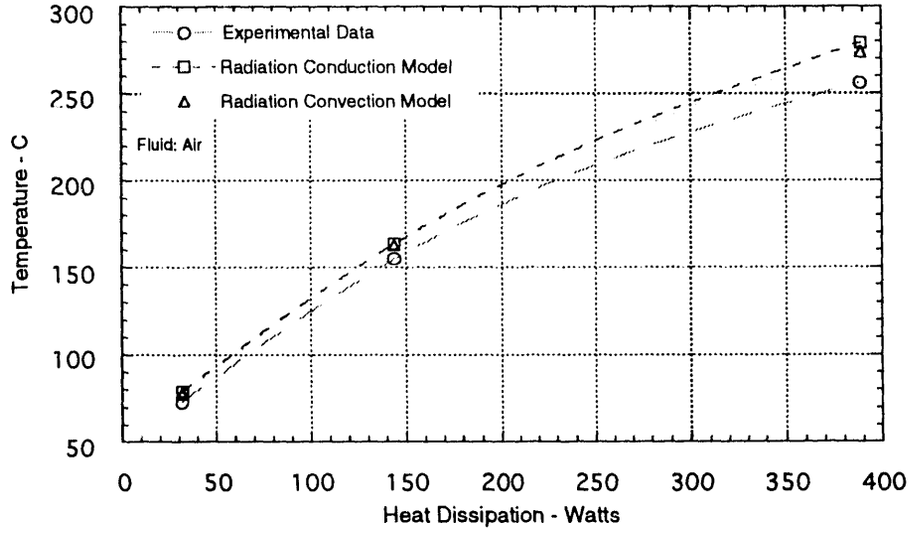

Figure 2. Thermal Model and Experimental Data Comparison with Air Fill Gas

Figure 2 shows a divergence between the predicted temperatures and experimental temperature data. Two factors are thought to account for the divergence, natural convection and axial conduction. As temperature increases, more heat is transferred by natural convection to the walls of the boundary box. This effect is not accounted for in the radiation conduction case and only partially in the radiation convection case. The radiation convection case accounts for natural convection from the rod array to the surrounding fluid but does not include any mass transport effects. The second effect is the axial conduction out the ends of the rods during the experiment. In that the numerical simulation is two-dimensional, end effects are not included. End effects cause the predicted temperatures to be higher than the experimental temperatures, and the effect is more noticeable at higher dissipation because the axial heat transfer driving potential is higher.

In Figures A1 through A6, an upward shift in temperature is noticeable in the experimental data. The calculated data shows a symmetric ring pattern with the hottest rods in the center. The asymmetry in the experimental temperature data indicates a natural convection heat transfer mechanism.

3.2 Helium Fill Gas

The maximum rod surface temperatures in the helium fill gas comparison, as shown in Figure 3, for the lowest heat dissipation, 109.8 W/m, are 73.0°C for the experiment, 72.7°C for the radiation conduction case, and 70.9°C for the radiation convection case. For the medium heat dissipation, 425.8 W/m, the maximum rod surface temperatures are 168.2°C for the experiment, 166.0°C for the radiation conduction case, and 162.4°C for the radiation convection case. At the highest heat dissipation, 939.5 W/m, the maximum rod surface temperatures are 236.8°C for the experiment, 252.4°C for the radiation conduction case, and 246.2°C for the radiation convection case.

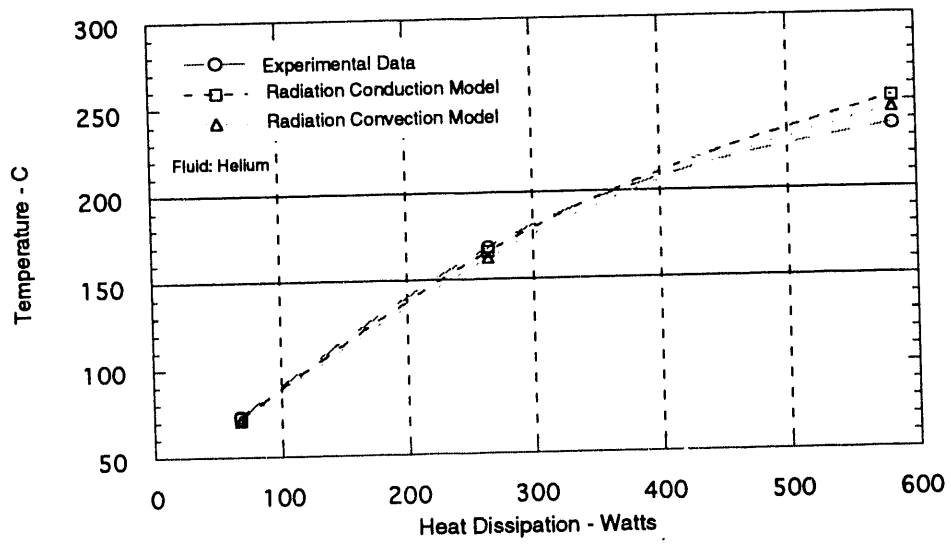

Figure 3. Thermal Model and Experimental Data Comparison with Helium Fill Gas

As in the air fill gas case, calculations with helium fill gas show divergence between the predicted temperatures and experimental temperatures as the heat dissipation increases. The explanation for the divergence in the helium fill gas case is thought to be the same as in the case using air.

In Figures B1 through B6, an upward shift in temperature is noticeable in the experimental data. The calculated data shows a symmetric ring pattern with the hottest rods in the center. The asymmetry in the experimental temperature data indicates a natural convection heat transfer mechanism.

3.3 Emissivity Sensitivity Study

The results of the emissivity sensitivity study are presented in Figure 4. There is a 13°C rise in maximum rod surface temperature for a 0.1 decrease in emissivity.

4.0 CONCLUSIONS

The numerically predicted temperatures are higher than the experimental data for all levels of heat dissipation with air as the fill gas. The temperature differences are 4°C and 23°C for the low heat dissipation and high heat dissipation, respectively.

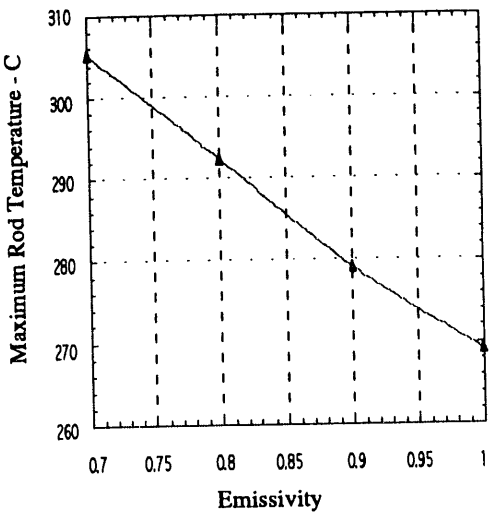

Figure 4. Emissivity Study Results

The temperature predictions using helium as a fill gas are lower for the low and medium heat dissipation level, but higher at the high heat dissipation. The temperature differences are 1°C and 6°C for the low and medium heat dissipation, respectively. For the high heat dissipation level, the temperature predictions are 16°C higher than the experimental data.

Convection effects are a second-order heat transfer mechanism for this problem. The experimental data indicates the presence of a natural convection heat transfer mechanism. However, convection effects contribute more to the temperature distribution of the rods and the location of the hottest rod surface temperature than to the maximum rod surface temperature. A conservative maximum rod surface temperature prediction is made by not including convection in the model. The conservative prediction is demonstrated because the radiation conduction models predict rod surface temperatures that are 1 to 6°C higher than the radiation convection model temperature predictions. However, if a rod surface temperature in a specific location needs to be predicted, including natural convection will increase the accuracy of the temperature prediction.

Differences between the predicted and experimental temperatures can be attributed to several factors. These factors include experimental uncertainty in the temperature and heat dissipation measurements, actual convection effects not included in the model, and axial heat flow in the experimental data.

This work demonstrates that horizontally oriented spent fuel rod surface temperature predictions can be made using existing commercial codes. A thermal analyst can predict horizontally oriented spent fuel rod maximum temperatures with commercially available codes and either the radiation conduction or radiation convection modeling approach. It also shows that end effects , such as axial heat transfer, will be increasingly important as the amount of dissipated heat increases.

5.0 REFERENCES

1. P/Thermal User Manual, PDA Engineering, Costa Mesa, CA, 1991.
2. Glass, R. E. et al., Standard Thermal Problem Set for the Evaluation of Heat Transfer Codes Used in the Assessment of Transportation Packages, SAND88-0380, Sandia National Laboratories, Albuquerque, NM, August 1988.
3. Lovett, P., and Todreas, N. E., An Experiment to Simulate the Heat Transfer Properties of a Dry, Horizontal Spent Nuclear Fuel Assembly, Masters Thesis, Massachusetts Institute of Technology, 1991.
4. Karlekar, B. V., and Desmond, R. M., Engineering Heat Transfer, West Publishing Co, 1977.

APPENDIX A

ROD ARRAY TEMPERATURE MAPS WITH AN AIR FILL GAS

Experimental

Calculated

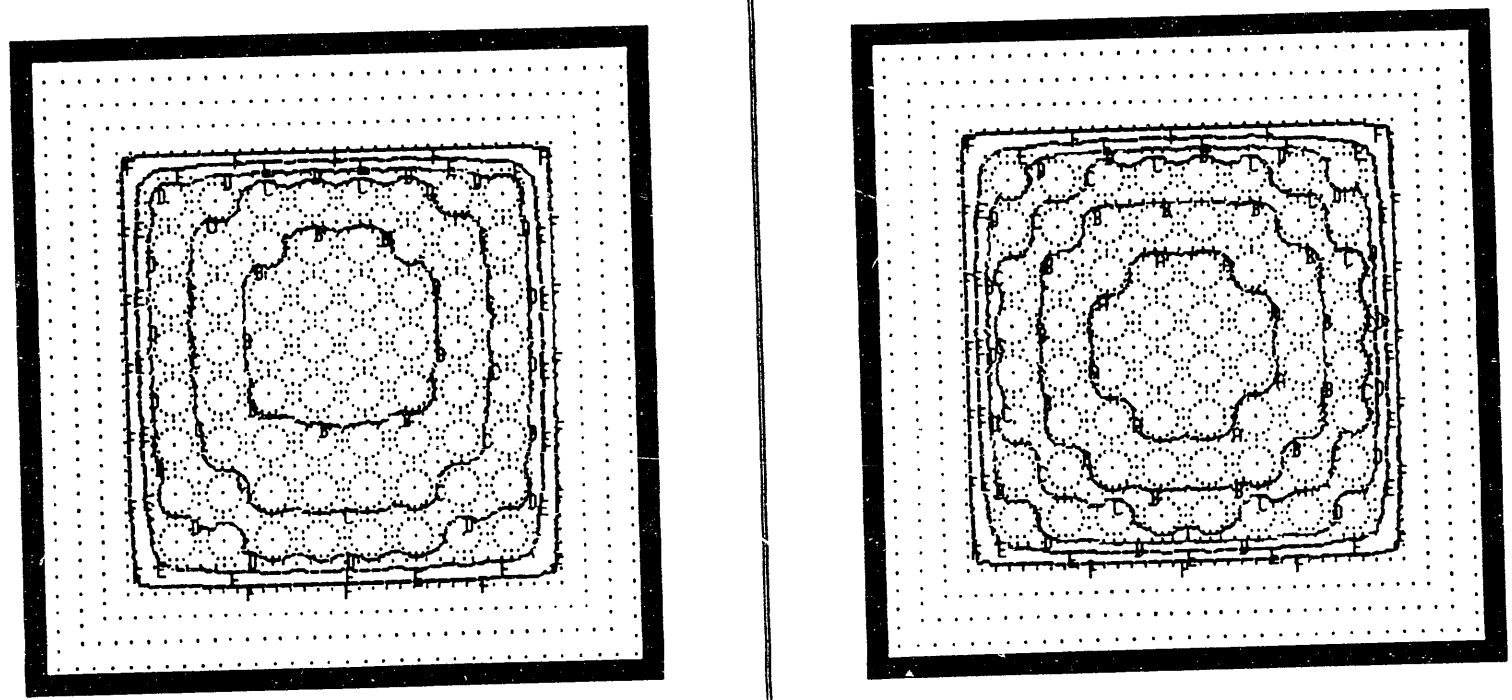

Legend: A=267.0; B=243.0; C=220.0; D=196.0;E=172.0; F=148.0
Note: All temperatures in degrees Celsius

Figure A1. Radiation Conduction, High Dissipation, Air Fill Gas

Experimental

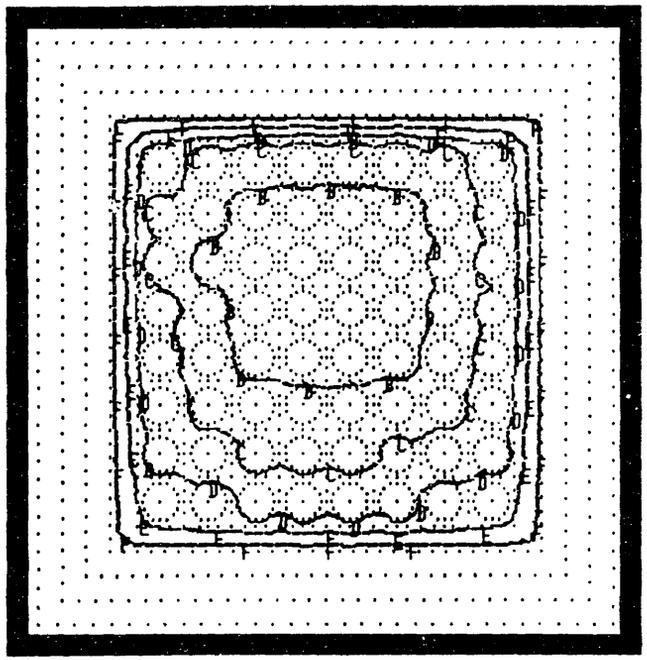

Calculated

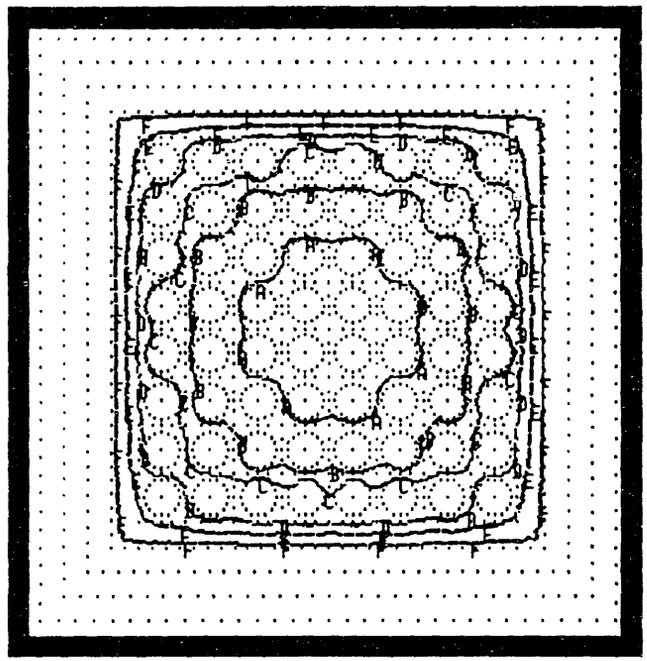

Legend: A=157.0; B=143.0; C=129.0; D=115.; E=102.0; F=87.7
Note: All temperatures in degrees Celsius

Figure A2. Radiation Conduction, Medium Dissipation, Air Fill Gas

Experimental

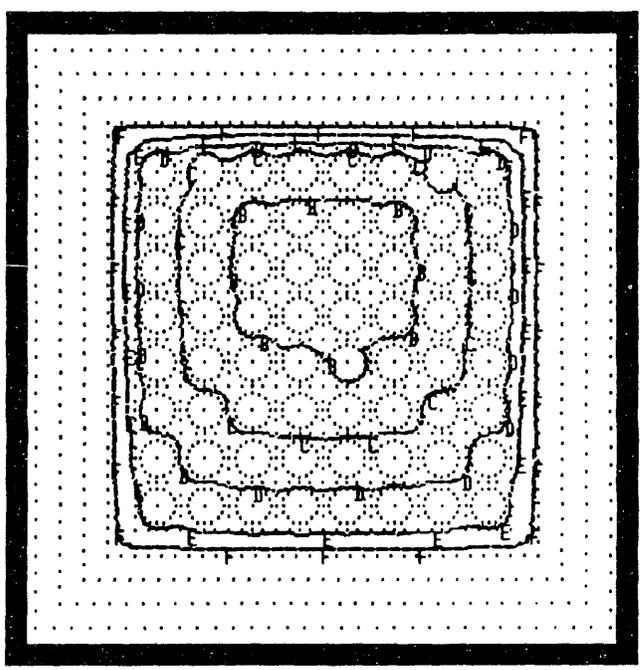

Calculated

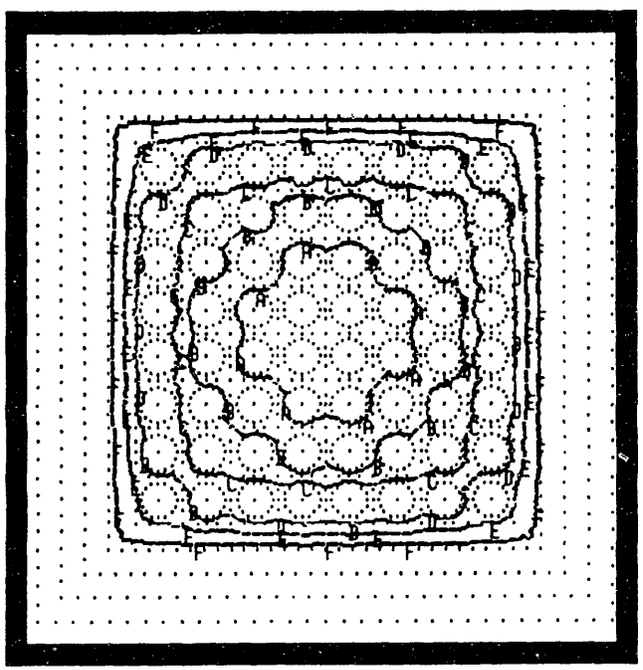

Legend: A=76.1; B=70.5; C=64.8; D=59.2; E=53.5; F=47.8
Note: All temperatures in degrees Celsius

Figure A3. Radiation Conduction, Low Dissipation, Air Fill Gas

Experimental

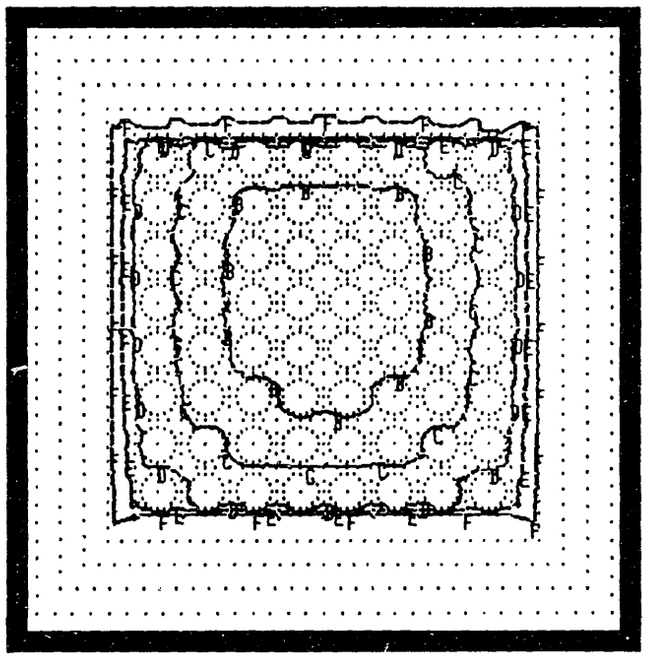

Calculated

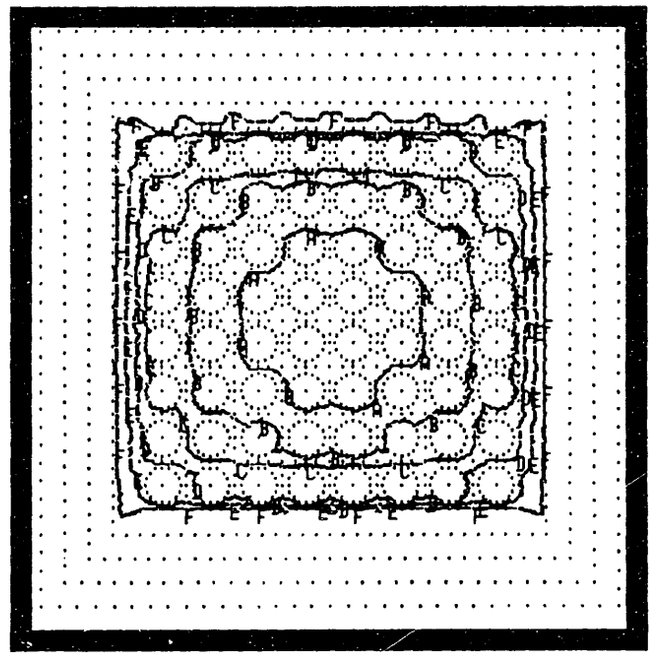

Legend: A=263.0; B=240.0; C=217.0; D=194.0;E=171.0; F=148.0
Note: All temperatures in degrees Celsius

Figure A4. Radiation Convection, High Dissipation, Air Fill Gas

Experimental

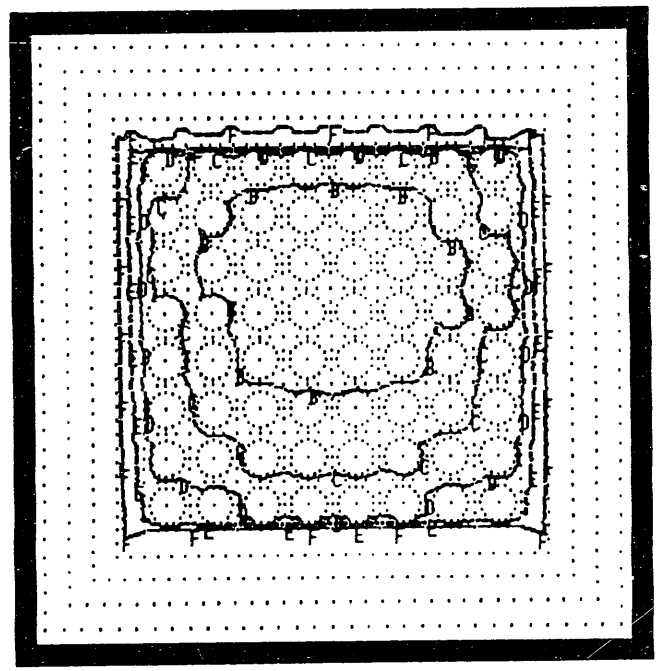

Calculated

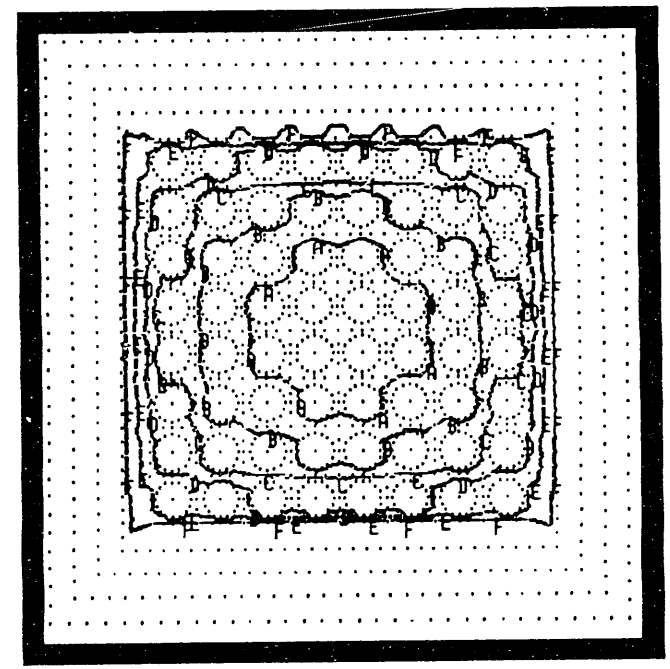

Legend: A=156.0; B=142.0; C=129.0; D=115.0;E=101.0; F=87.6
Note: All temperatures in degrees Celsius

Figure A5. Radiation Convection, Medium Dissipation, Air Fill Gas

Experimental

Calculated

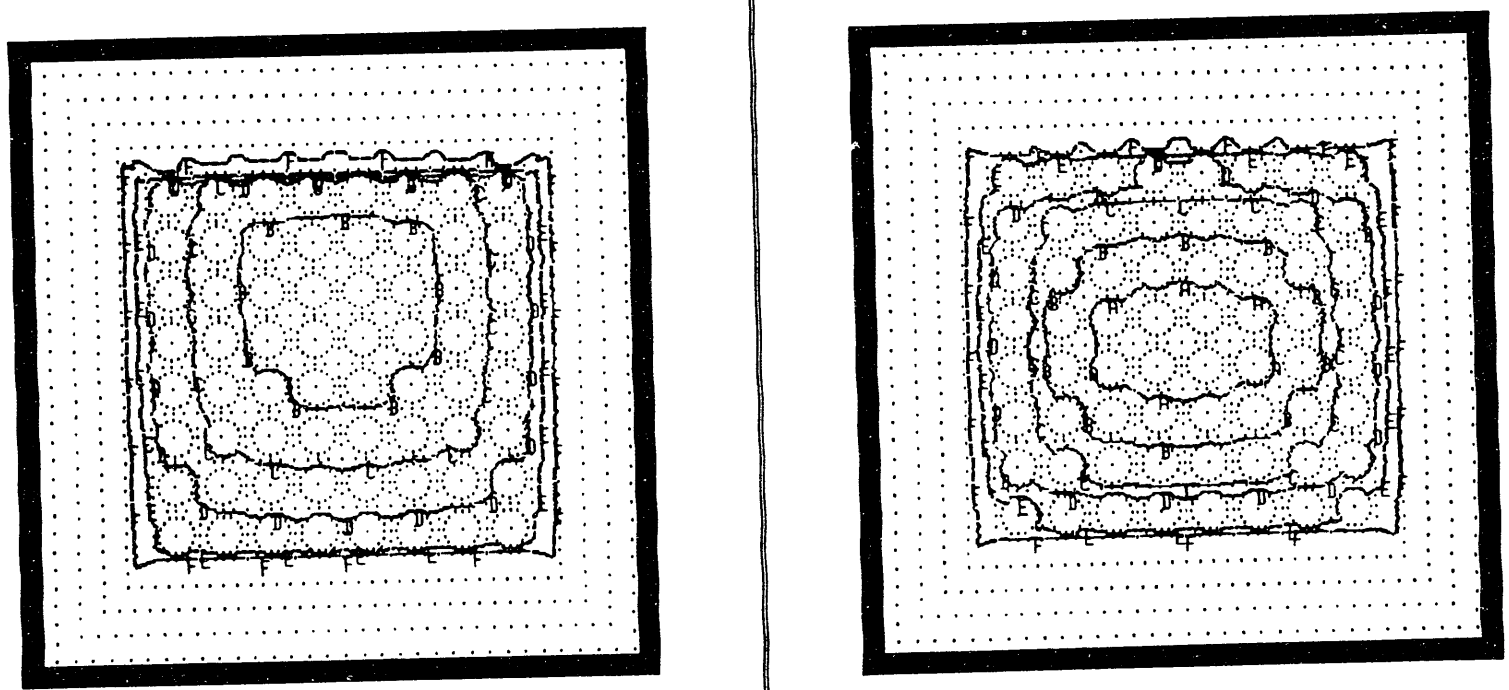

Legend: A=75.0; B=69.6; C=64.1; D=58.6; E=53.2; F=47.7
Note: All temperatures in degrees Celsius

Figure A6. Radiation Convection, Low Dissipation, Air Fill Gas

APPENDIX B

ROD ARRAY TEMPERATURE MAPS WITH A HELIUM FILL GAS

Experimental

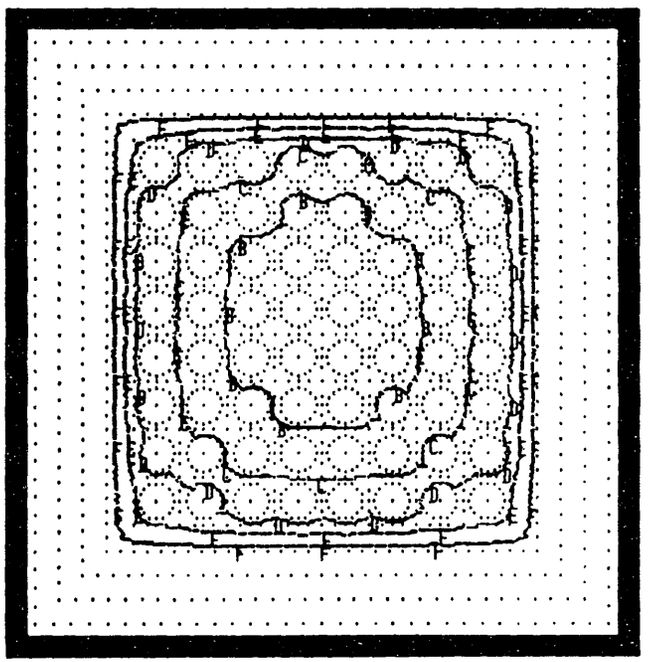

Calculated

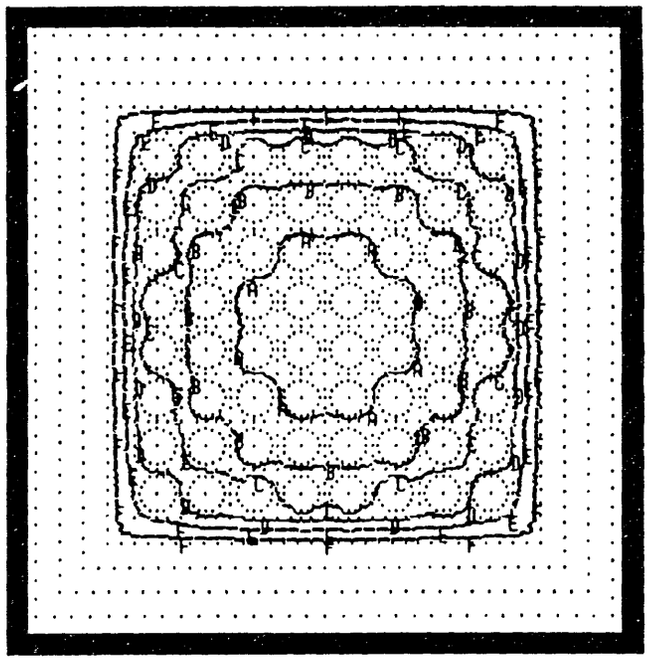

Legend: A=242.0; B=221.0; C=200.0; D=179.0;E=158.0; F=138.0
Note: All temperatures in degrees Celsius

Figure B1. Radiation Conduction, High Dissipation, Helium Fill Gas

Experimental

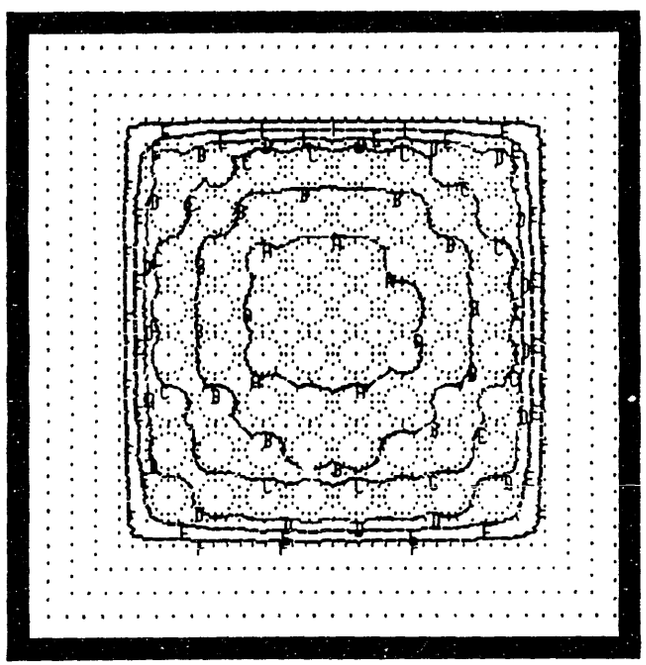

Calculated

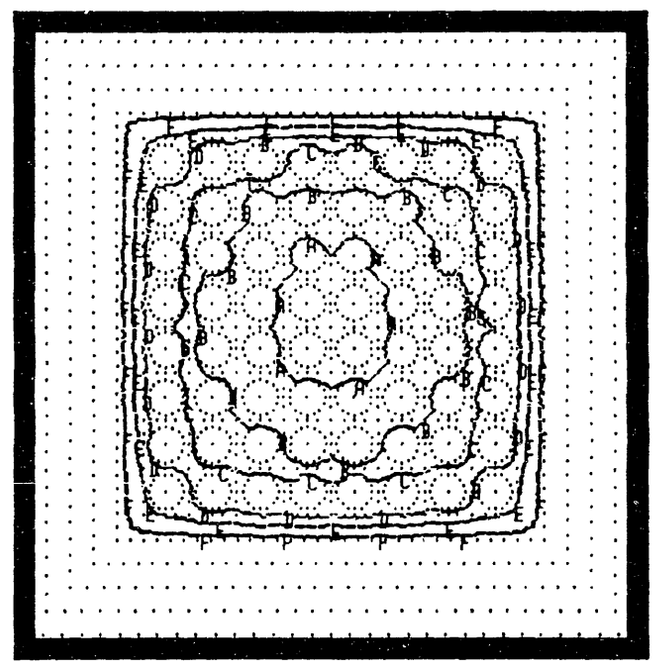

Legend: A=162.0; B=149.0; C=137.0; D=125.0; E=112.0; F=100.0
Note: All temperatures in degrees Celsius

Figure B2. Radiation Conduction, Medium Dissipation, Helium Fill Gas

Experimental

Calculated

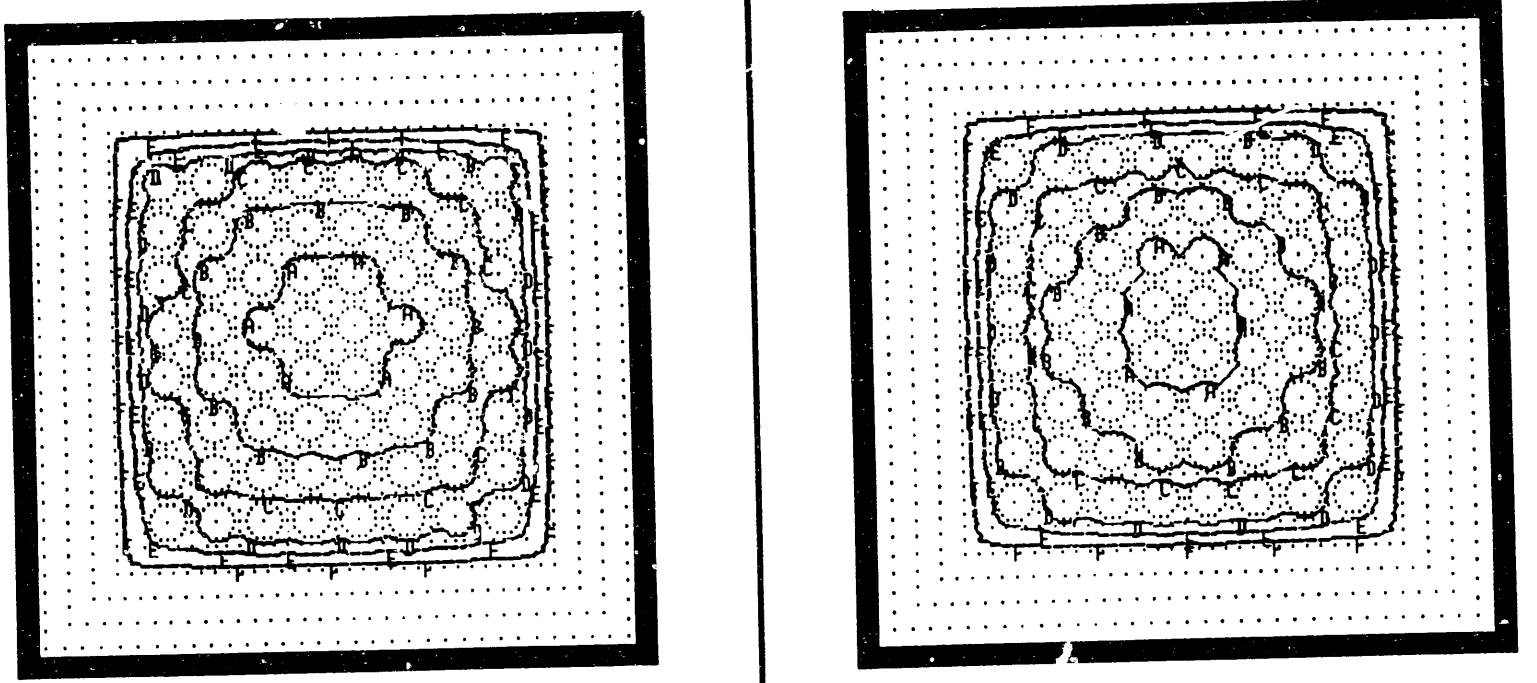

Legend: A= 71.1; B= 66.8; C= 62.5; D= 58.2; E= 53.9; F= 49.6
Note: All temperatures in degrees Celsius

Figure B3. Radiation Conduction, Low Dissipation, Helium Fill Gas

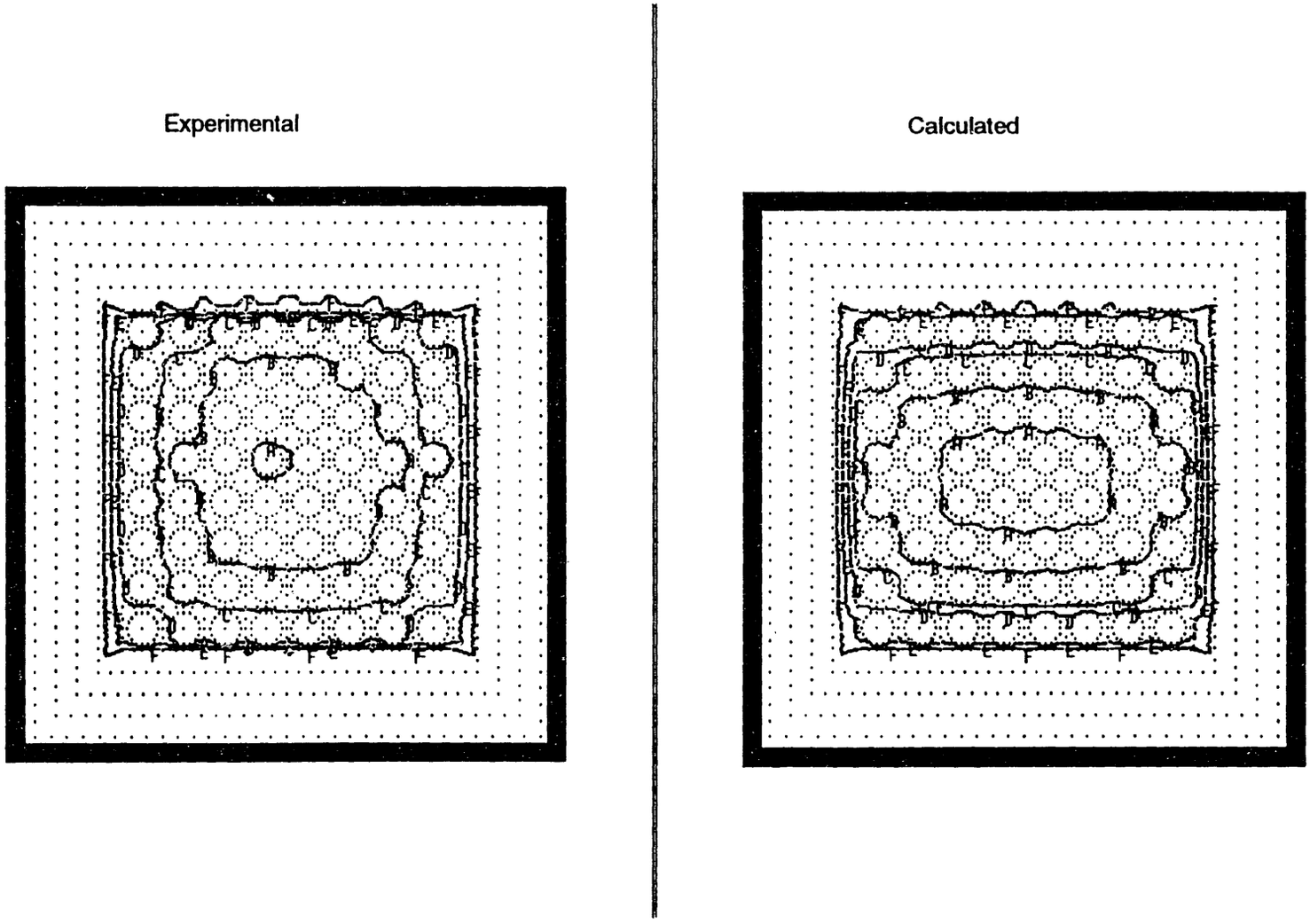

Legend: A=236.0; B=217.0; C=197.0; D=177.0; E=157.0; F=137.0
Note: All temperatures in degrees Celsius

Figure B4. Radiation Convection, High Dissipation, Helium Fill Gas

Experimental

Calculated

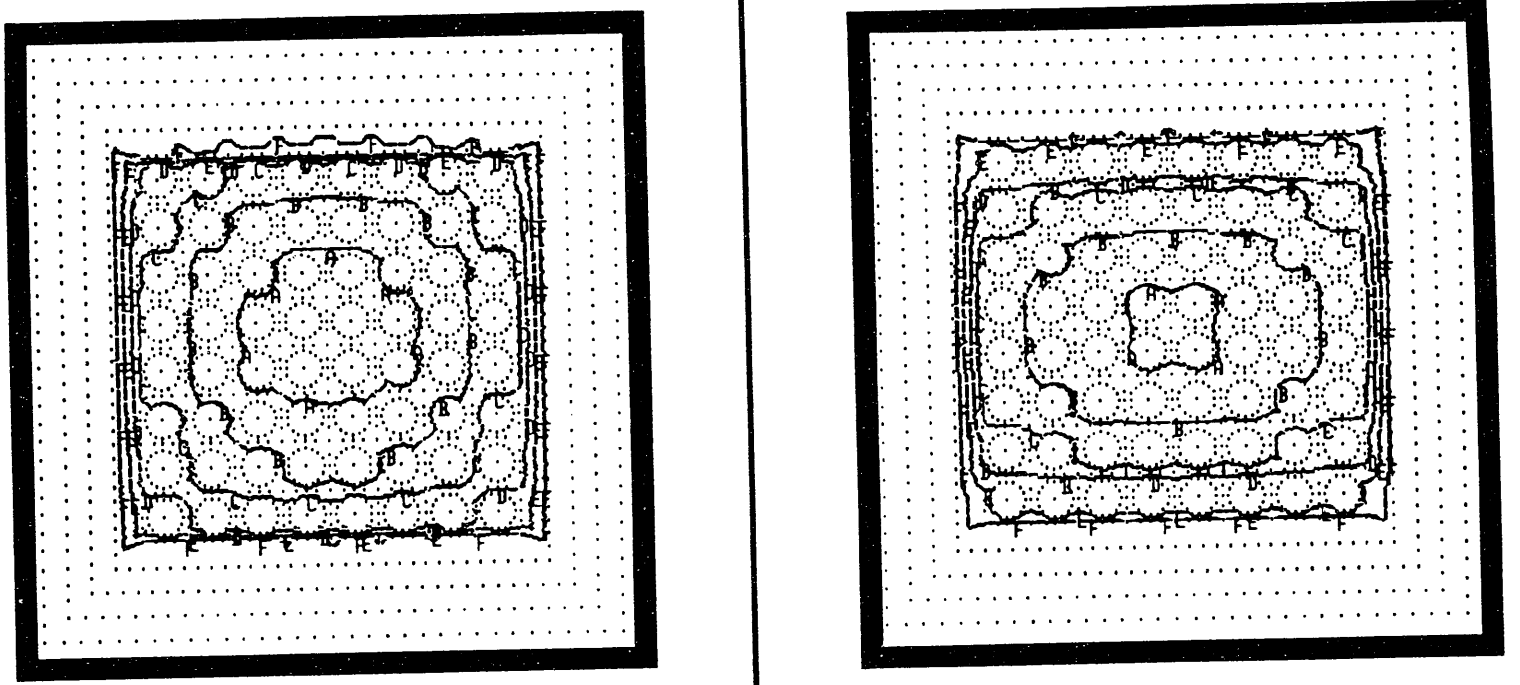

Legend: A=162.0; B=150.0; C=137.0; D=125.0; E=113.0; F=100.0
Note: All temperatures in degrees Celsius

Figure B5. Radiation Convection, Medium Dissipation, Helium Fill Gas

Experimental

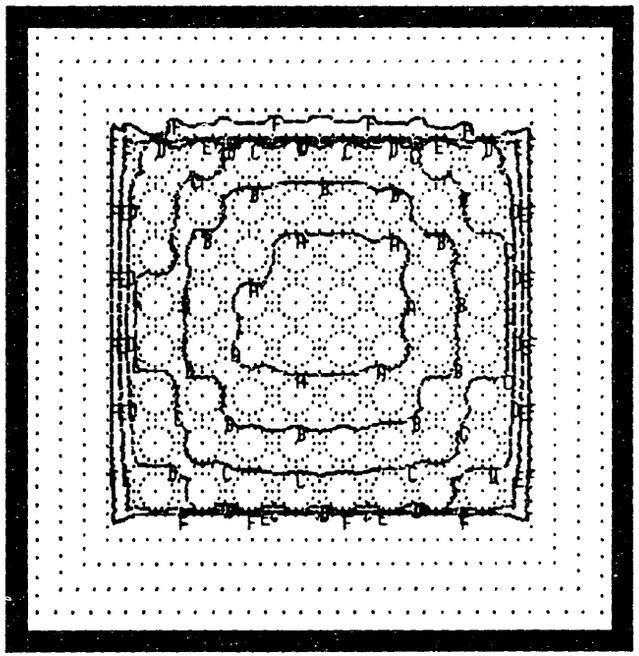

Calculated

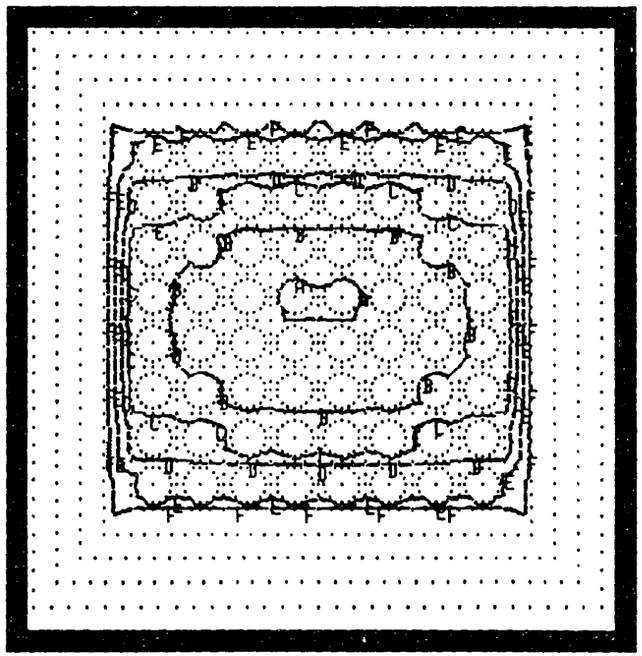

Legend: A=70.8; B=66.5; C=62.2; D=57.8; E=53.5; F=49.2
Note: All temperatures in degrees Celsius

Figure B6. Radiation Convection, Low Dissipation, Helium Fill Gas

DISTRIBUTION

Knolls Atomic Power Laboratory (10)
General Electric
P.O. Box 1072
Schenectady, NY 12301
Atn: D. M. Basttiste

U.S. Department of Energy (5)
EM-561
Trevion II
Washington, DC 20585-0002
Attn: L. Blalock
E. McNeil
M. Conroy

U.S. Department of Energy (3)
Washington, DC 20585-0002
Attn: J. Williams, RW-321
W. Lake, RW-323

U.S. Department of Energy
Office of Security Regulations
Washington, DC 20545
Attn: M. Wangler, EH-32

U.S. Department of Energy (2)
Idaho Operations Office
550 Second Street
Idaho Falls, ID 83401
Attn: M. Fisher
K. Svinicki

Sandia Distribution:

1513	V. F. Nicolette
6000	D. L. Hartley
6600	J. B. Woodard
6603	R. E. Luna Attn: TTC Master File
6603	TTC Library (5)
6641	R. P. Sandoval
6642	G. F. Hohnstreiter
6642	K. B. Sorenson
6642	J. A. Koski
6642	S. D. Wix (5)
6643	T. L. Sanders
6643	S. E. Gianoulakis
7141	Technical Library (5)
7151	Technical Publications
7613	Document Processing for for OSTI (10)
8523-2	Central Technical Files

DATE
FILMED
9/21/93
END